**Rotational migration in human pancreatic ductal organoids depends on actin and myosin activity**.

Gengqiang Xie[1], Yue Julia Wang[1], D. Thirumalai[2], Xin Li[2]*, Jerome Irianto[1]*

[1]Department of Biomedical Sciences, College of Medicine, Florida State University, Tallahassee, FL 32306

[2]Department of Chemistry, University of Texas at Austin, Austin, TX 78712; Department of Physics, University of Texas at Austin, Austin, TX 78712

*co-corresponding author:
Jerome Irianto, Phone: 850-645-9438, Email: jerome.irianto@med.fsu.edu
Xin Li, Phone: 832-701-3379, Email: xinlee0@gmail.com

**Abstract**

Rotational migration is one specific form of collective cell migration when epithelial cells are confined in a spherical geometry, such as in the epithelial acini. This tissue-level rotation motion is crucial for the morphogenesis of multiple epithelial systems. Here, we introduce a new primary human model for the study of rotational migration, pancreatic ductal organoids. Live imaging revealed the persistent rotation of the organoids over time. By tracking the nuclei, the three-dimensional trajectory of the cellular movement was reconstructed and the velocity of the rotation was quantified. The presence of focal adhesion clusters and prominent actin stress fibers were observed at the basal side of the organoids, suggesting the interactions between the cells and the surrounding extracellular matrix. Finally, our inhibition study showed the dependence of pancreatic ductal organoid rotational migration on myosin activity, actin polymerization, and actin branching. We hope that this model will enable future studies with human primary cells, which are more faithful to normal epithelial cells.

## Introduction

The collective migration of epithelial cells plays a vital role in many biological processes, including morphogenesis, wound repair, tissue homeostasis, and cancer metastasis[1]. One specific form of collective migration is rotational migration, which is observed when epithelial cells are confined in a spherical geometry. In rotational migration, the entire multicellular structure rotates as a result of directed collective migration. This migration mode has been observed in various systems, such as the follicle cells of *Drosophila* egg chambers[2-6], canine kidney epithelial acini[7-9], murine pancreatic organoids[10,11], and human mammary acini[12-14]. This suggests that rotational migration is an inherent dynamic feature of three-dimensional multicellular structures. Moreover, the significant role of rotational migration in morphogenesis has been reported in several studies. For example, disruption of *Drosophila* follicle cells' rotational migration prevented the elongation of the egg chamber[15,16], a critical step in its developmental process. Recent work in human mammary gland morphogenesis has also revealed that rotational migration is needed for the budding of spherical alveoli from the mammary duct network[17]. Furthermore, the loss of rotational migration was associated with the malignant behavior of breast cancer cells[12,13], suggesting the potential role of rotational migration in maintaining normal tissue homeostasis.

To establish the collective rotational migration, the epithelial cells need to collectively polarize towards the migration direction. Interestingly, unlike other collective cell migration, polarizing external cues such as space or chemical gradient are not available in rotational migration. Hence, the polarization process is likely to rely on cell-to-cell or cell-to-extracellular matrix (ECM) interactions. Several studies using the invertebrate *Drosophila* follicle cell model have identified a number of these polarizing cell-cell interactions. The accumulation of cadherin protein Fat2 at the trailing edge of a follicle cell is essential for the polarization of the WAVE complex at the leading edge of the adjacent cell[2]. In another study, they showed the roles of formin protein DAAM and Rho GTPase Cdc42 in actin stress fibers and protrusions polarization[3,4]. For the mammalian systems, on the other hand, the cellular polarization mechanisms are still unknown. Nevertheless, perturbation of some key players, such as actomyosin contractility[8,12,13,18], cell-cell junction protein E-cadherin[18], ECM receptor integrin β1[12,13], signaling proteins EGFR[12], and β-catenin[9], has been shown to disrupt the rotational migration in mammalian models. However, most of the findings were established in cell lines. In our opinion, the study of rotational migration regulation will benefit from primary human models, derived from human tissues and more faithful to normal epithelial cells. This will potentially provide more accurate findings on epithelial cell behavior and biology. Recent developments in organoid culture systems open the door for *in vitro* primary human

models, such as in the brain[19], intestine[20], pancreas[21], and others[22,23].

In this study, we introduce a new human model for rotational migration study, the pancreatic ductal organoids, which were derived from human exocrine tissues. Upon culture in Matrigel, the pancreatic ductal epithelial cells form a cystic structure consisting of a spherical lumen encapsulated by a single layer of epithelial cells. Live imaging revealed the persistent rotation of the organoids over time. By tracking the nuclei, we reconstructed the trajectory of the cellular movement and quantified its velocity. We also observed the presence of focal adhesion clusters and prominent actin stress fibers at the basal side of the organoids, suggesting the interactions between the cells and the surrounding Matrigel. Finally, our inhibition study showed the dependence of pancreatic ductal organoid rotational migration on myosin activity, actin polymerization, and actin branching.

## Results and discussion

### Rotation of human pancreatic ductal organoid.

Normal human pancreatic ductal organoids were derived from the exocrine tissue provided by the Integrated Islet Distribution Program (IIDP). By culturing the exocrine tissue in Matrigel, the ductal cells will grow and establish a spherical structure that consists of a lumen surrounded by a thin layer of epithelial cells (**Figure 1A**)[21,24]. Apicobasal polarity was observed within these cells, where the immunostaining of the apical marker ZO-1 was observed at the lumen side, while the basal marker integrin α6 (ITGA6) was observed between the cells and at the outer side of the cells, which is in contact with the surrounding Matigel. Moreover, continuous staining of the tight junction protein ZO-1 can be observed between the cells at the apical side (**Figure 1B**), suggesting an intact barrier function of the epithelial layer. The cystic morphology of the pancreatic ductal organoid is also another evidence of the functional epithelial barrier. Lumen formation is initiated by the secretion of ions (such as the sodium cation and chloride anion) into the luminal space, which increases the luminal osmolality and in turn, drives the influx of water and the increase in lumen volume[25-27]. Hence, the maintenance of this cystic morphology is highly dependent on the epithelial barrier function that preserves the osmotic gradient.

Brightfield live imaging of the pancreatic ductal organoids revealed the rotational motion of the organoids over time (**Video 1**). To investigate the rotation further, the nuclei were stained with a non-toxic, cell-permeable, and highly specific live cell DNA probe, SPY650-DNA, followed by live

imaging using spinning disk confocal microscopy. Indeed, we observed the directed motion of the nuclei that resulted from the rotation of the whole organoid (**Figure 1C, Video 2**). We observed two key differences between the observed rotation of our pancreatic ductal organoids, MDCK (canine kidney), and MCF10A (human mammary) spheroids. One, rotation in MDCK and MCF10A spheroids is limited to the early, low cell-number stages (<20 cells)[7,12,13], whereas rotation in the pancreatic ductal organoids can still be observed in large organoids (>300 µm in diameter, **Video 1**) that consist of hundreds of cells. Two, rotation in MDCK cells at later stages that involve more cells (>20 cells) is only observed in a gradient of Matrigel concentrations[8,9] – making it a form of durotaxis – whereas the rotation we observed in the pancreatic organoids is within a homogeneous Matrigel matrix.

As a comparison, we also looked into the pathological pancreatic ductal adenocarcinoma (PDAC) organoids. Similar to their normal counterpart, PDAC organoids also have a cystic morphology and the apicobasal polarity is intact (**Figure S1A**). However, the PDAC cells tend to have cuboid cellular morphology, resulting in a cell layer that is thicker and denser than the normal pancreatic ductal organoid. Moreover, stratified cell layers are occasionally observed within the PDAC organoids. To our surprise, the rotational migration phenotype is lost in the PDAC organoids (**Figure S1B, Video 3**), suggesting the potential importance of rotational migration in maintaining normal tissue homeostasis. This observation is also in line with previous studies in breast cancer[12,13].

**Quantification of human pancreatic ductal organoid rotation.**

Tracking the movement of single cells within large organoids in three dimensions remains a significant challenge. To quantify the organoid rotational migration, live imaging data of the nucleus was processed using a deep learning segmentation method and custom tracking algorithms (see Materials and methods). This image-processing pipeline allows us to reconstruct the nucleus positions over time and derive the displacement trajectory of each nucleus within the rotating organoid (**Figure 2A-C**). Next, the velocity of each nucleus at the organoid surface at a given time point was calculated by dividing the displacement by the time covered between the imaging time points. The average velocity is relatively stable over the imaging period (**Figure 2D**). Looking at the velocity distribution, the velocity ranges between 0 to 30 µm/hr, with a peak at around 15 µm/hr (**Figure 2E**). Measurements on more pancreatic ducal organoids reveal that the average velocity ranges between ~15 and ~18 µm/hr (**Figure 2F**). This rotation velocity falls within the range of velocity reported in other rotational migration models, including the *Drosophila* follicle

cells at 12 to 36 µm/hr, the murine pancreatic organoid at around 12 µm/hr, the canine kidney epithelial line MDCK at 5 to 20 µm/hr[9], and the human breast epithelial line MCF10A at 12.5 to 17.5 µm/hr[13]. In contrast, the trajectory reconstruction of the PDAC organoids showed that the nuclei are moving randomly within a limited region, at an average velocity of about 3 µm/hr (**Figure S1C-F**).

**Pancreatic ductal organoid rotational migration relies on actomyosin contractility.**

Next, we pondered how the pancreatic ductal cells migrate along the organoid rotational axis. The apical side of the organoid interacts with the fluid-filled luminal space, hence, it is less likely that the cells are migrating on the apical side. On the other hand, the basal side interacts with the Matrigel, and the cells can interact with the ECM proteins through the integrins and migrate on this interface. Indeed, we observed clusters of focal adhesion protein paxillin and prominent actin stress fibers at the basal side of the organoids (**Figure 3A**), indicative of cell-ECM adhesions. Moreover, we also observed the enrichment of the phosphorylated myosin regulatory light polypeptide 9 (pMYL9) on the actin stress fibers (**Figure 3B**), suggesting the activation of non-muscle myosin IIA and actomyosin contractility. This is in line with the findings in the rotating *Drosophila* follicle cells, where paxillin clusters and myosin-decorated actin fibers were also observed at the basal side of the follicle cells[3]. These observations suggest the potential involvement of actomyosin activity in regulating rotational migration.

To investigate the role of myosin contractility, the pancreatic ducal organoids were treated with a small molecule myosin II inhibitor, Blebbistatin that has a high affinity towards the myosin-ADP-Pi complex and locks the myosin in an actin detached state[28]. Nuclei live imaging was performed before and after the Blebbistatin treatment on the same organoid (**Figure 4A, Video 4**). From the trajectory analysis (**Figure 4B**), we observed a significant slowdown of the rotation while the rotational direction was more or less maintained. Averaging the quantified velocity over the imaging period clearly showed a significant decrease in velocity after the Blebbistatin treatment (**Figure 4C-D**). This suggests the reliance of rotational migration on myosin contractility. To note, myosin inhibition does not compromise the luminal structure of the organoid, where the apicobasal polarity was intact and we still observed the continuous tight junction network at the apical side (**Figure S2A-B**). Looking closer at the basal side of the Blebbistatin-treated organoids, we observed significant disruption of the actin stress fibers and the accumulation of pMYL9 at the base of the actin fibers (**Figure 4E**). Instead of the long and relatively straight actin stress fibers

observed in the untreated organoids (**Figure 3**), the actin fibers tend to have wavy morphology (**Figure 4E**) and are shorter after the Blebbistatin treatment (**Figure S2C**).

**Rotational migration also depends on actin branching activity.**

The results above pointed towards the critical role of actin organization on pancreatic ductal organoid rotational migration. To study this, we treated the organoids with an actin polymerization inhibitor, Latrunculin A. Indeed, inhibition of actin polymerization significantly slows down the organoid rotation (**Figure 5A**). Similar to the Blebbistatin-treated organoids, Latrunculin A treatment does not disrupt the apicobasal polarity of the organoids (**Figure S3A**). However, we observed wavy patterns of the tight junction proteins ZO-1 (**Figure S3B**), which were not observed in the untreated and Blebbistatin-treated organoids. These wavy tight junction structures might imply a decrease in cellular tension at the apical side of the Latrunculin A treated cells. Looking closer to the basal side, Latrunculin A treatment seems to drive the actin distribution towards the perimeter of the cells, causing the enrichment of actin at the cell-cell boundaries (**Figure 5B**). Additionally, the enrichment of activated myosin (pMYL9) was also observed at the periphery of some cells.

Next, we looked into actin branching, an essential process in actin filament assembly and organization. The branching of actin is crucial for the formation of lamellipodium[29], a broad and flat cellular protrusion at the leading edge of migrating cells. The rotating *Drosophila* follicle cells form lamellipodia as well, they form at the leading edge of the cells and protrude below the adjacent cells -- a structure called the cryptic lamellipodia[2,30]. By imaging the cell-cell junction protein E-cadherin, we also observed cryptic lamellipodia in the pancreatic ductal organoids (**Figure S3C**), implying that actin branching is likely to play a role in pancreatic ductal organoid rotational migration. To test this, we treated the organoids with an Arp2/3 inhibitor, CK-666[31]. The nucleation of actin branching relies on the assembly of the Arp2/3 complex at the actin filaments[32], hence its inhibition will prevent actin branching. The CK-666 treatment significantly slows down the pancreatic ductal organoid rotation (**Figure 5C**). However, in contrast to the Blebbistatin and Latrunculin A treatment, we still observed prominent actin stress fibers at the basal side of the CK-666 treated organoids, and some of the fibers were decorated with the active pMYL9 (**Figure 5D**). These findings confirm the dependence of pancreatic ductal organoid rotational migration on actin branching activity, and potentially orthogonal from the role of myosin contractility.

In summary, we have revealed a new primary human model to study epithelial cell rotational migration -- the pancreatic ductal organoids. As an effort to characterize this model system, we quantified the velocity of the rotation and showed that the organoid rotational migration depends on myosin contractility, actin polymerization, and actin branching. The method developed here for tracking single-cell movement in three dimensions across large organoids can also be applied to other experimental systems. However, the regulatory mechanisms of epithelial cell rotational migration are still largely unknown, for example, what are the mechanisms underlying the initiation of rotational migration? Once the rotational migration is established, what are the regulatory mechanisms that maintain the collective migration over time? Moreover, what are the downstream signaling pathways and functional processes that rely on rotational migration? We hope that the introduction of this model will contribute to future studies on rotational migration regulation and also potentially increase the accuracy of future findings by enabling investigations using primary cells derived from human tissues, which are more faithful to normal epithelial cells. Typically, the pancreatic ductal organoids can be passaged at a 1:2 expansion ratio weekly, hence, with adequate planning, the organoids should enable rapid experimentations. Additionally, the organoids can be genetically modified through either lentiviral or adenoviral transduction, making them suitable for in-depth mechanistic studies. However, it is important to note that the culture media of the pancreatic ductal organoids contains growth factors, hormones, and other supplements that might impact rotational migration. For example, A83-01 and mNoggin inhibit TGF-β signaling, while R-spondin1 and Wnt3a promote the activation of Wnt signaling. TGF-β signaling pathway has been shown to regulate cell migration[33,34] and the impact of TGF-β inhibition on the organoid rotational migration is unclear. However, we have previously excluded the inhibitors of TGF-β from the culture media and we still observed the organoid rotational migration. Nevertheless, it is crucial to consider the culture condition of these organoids when interpreting the experimental findings. Another interesting aspect to consider is that in the rotating organoid, the epithelial ductal cells are not simply migrating on a two-dimensional surface. Instead, they are migrating within a more complex spherical tissue structure with a lumen at the center of it. The lumen is a pressurized system[25,35], hence the apical side of the epithelial ductal cells should experience a level of hydrostatic pressure. Mechanical cues by hydrostatic pressure have been shown to regulate cellular phenotype[35-37], making us wonder whether luminal pressure has a role in regulating organoid rotational migration. Furthermore, surface curvature has been shown to influence cellular behavior too[38], implying the potential role of the organoid spherical surface on rotational migration.

## Materials and methods

### Pancreatic ductal organoid culture

Normal human pancreatic ductal organoids were derived from pancreatic exocrine tissues isolated from cadaver donors (RRID: SAMN17277513 and SAMN38518868), which were acquired through the Integrated Islet Distribution Program (IIDP). IIDP provided 0.5 mL exocrine tissue, which is equal to ~20 million cells. The exocrine cells were seeded into Matrigel (Corning) to allow for the growth and expansion of pancreatic ductal organoids. The Matrigel culture and expansion of pancreatic ductal organoids were performed following the Tuveson Laboratory Murine and Human Organoid Protocols (http://tuvesonlab.labsites.cshl.edu/wp-content/uploads/sites/49/2018/06/20170523_OrganoidProtocols.pdf), which were kindly compiled based on that lab's their previous studies[21,24]. The human wash media and complete feeding media were used, as suggested by the Tuveson Lab protocol. The wash media consists of Advanced DMEM/F-12 (ThermoFisher), supplemented with 10mM HEPES (ThermoFisher), 1X GlutaMAX supplement (ThermoFisher), 100 µg/mL Primocin (Invivogen), and 0.1% BSA (ThermoFisher). The complete feeding media consists of Advanced DMEM/F-12, supplemented with 10mM HEPES, 1X GlutaMAX supplement, 100 µg/mL Primocin, 1X Wnt3a conditioned media (refer to Tuveson lab protocol), 1X R-spondin1 conditioned media (refer to Tuveson lab protocol), 1X B27 supplement (ThermoFisher), 10mM Nicotinamide (Sigma), 1.25mM N-acetylcysteine (Sigma), 100 ng/mL mNoggin (Peprotech), 50 ng/mL hEGF (Peprotech), 100 ng/mL hFGF (Peprotech), 10nM hGastrin I (Tocris), 500nM A83-01 (Tocris), and 1µM PGE2 (Tocris). Considering the cells doubling time, the organoids were passaged 1:2 every 10 to 14 days. For the passage procedure, the organoid containing Matrigel domes was mechanically disrupted by pipetting the complete media up and down within the well plate. The cell suspension was transferred to a 5 mL protein LoBind tube (Eppendorf) and centrifuged at 200xg, 4$^{o}$C for 5 minutes. The supernatant was aspirated and the cell pellet was resuspended in ice-cold wash media, followed by centrifugation at 200xg, 4$^{o}$C for 5 minutes. The supernatant was aspirated and the cell pellet was resuspended in ice-cold Matrigel. The Matrigel cell suspension was pipetted onto a pre-warmed well plate (~37$^{o}$C) to form the Matrigel domes containing the pancreatic ductal cells. Due to the growth limitation of the human pancreatic ductal organoid, the experiments were done on organoids with passage numbers less than 10. The primary tumor PDAC organoids were acquired from ATCC, as part of the Human Cancer Models Initiative, with the organoid name HCM-CSHL-0092-C25. The culture procedure of the PDAC organoids was very similar to the normal pancreatic ductal organoid culture described above, except for the exclusion of PGE2 in

the complete feeding media. For the inhibitor study, the organoids were treated with either 200 µM Blebbistatin (Sigma), 1 µM Latrunculin A (VWR), or 200 µM CK-666 (MedChemExpress). For live imaging, the organoids were treated for 1 hour before the post-treatment live imaging. For the immunofluorescence imaging, the organoids were treated for 12 hours before fixation.

**Immunofluorescence imaging**

Pancreatic ductal organoids within the Matrigel domes were fixed in 4% formaldehyde (EMS) for 15 min, permeabilized by 0.5% Triton-X (Sigma) for 10 min, blocked by 5% BSA (VWR), and incubated overnight in the primary antibodies against ZO-1 (ThermoFisher #61-7300), ITGA6 (EMD Millipore #MAB1378), phosphorylated MYL9 (pSer19) (ThermoFisher #MA5-15163), MYH9 (Proteintech #11128-1-AP), Paxillin (Abcam #ab32084), ITGB1 (DSHB #AIIB2), or E-cadherin (CellSignaling #3195S). The samples were incubated in the corresponding Alexa Fluor secondary antibodies (ThermoFisher) for 1.5 hours. DNA was stained with 2 µg/mL DAPI (Sigma) for 15 min. Actin filaments were stained with 1 µg/mL Phalloidin-TRITC (Sigma) for 1 hour. Confocal imaging was done using a Zeiss LSM 880 system with a 63X/1.4 NA oil immersion objective.

**Live imaging**

For the live imaging of the nuclei, the pancreatic ductal organoids within the Matrigel domes were stained with 1X SPY650-DNA (Cytoskeleton) for 16 hr prior to the live imaging. SPY650-DNA was present throughout the live imaging. Live imaging was performed using an Andor Revolution Spinning Disk Confocal system (Oxford Instruments) with either 20X/0.75 NA or 40X/0.8NA objectives, within an incubator chamber maintained at 37ºC and 5% $CO_2$. Z-stack images were taken every 30 minutes with a z-distance of 2 µm between each stack. Meanwhile, the brightfield live imaging was performed using an Olympus IX71 with a digital sCMOS camera (Prime 95B, Photometrics) and a 10X/0.3 NA objective, within an incubator chamber maintained at 37ºC and 5% $CO_2$.

**Image processing and velocity quantification**

To acquire the position of the nuclei, each of the confocal z-stack images was subjected to the tracking and segmentation algorithms TrackMate v.7.14.0[39] and StarDist v.0.9.1[40] within Fiji v.2.15.1[41]. The TrackMate-StarDist analysis provides the x, y, and z locations of the detected nuclei segments, and represents each continuous nucleus segment along the z-stack as a single track. Hence, a track of nucleus segments detected here represents one individual nucleus. Next, by using an in-house MATLAB (MathWorks) algorithm, the mid-z location of each nucleus was

determined by recording the location of the nucleus segment with the highest mean intensity along each track. At this point, each nucleus of a given confocal z-stack image was represented by an x-y-z coordinate. Finally, the trajectory tracking of the nuclei over time was done by using the particle tracking algorithm[42], which was adapted into MATLAB. The velocity of each nucleus was calculated from the displacement along the trajectory divided by the time needed to cover the distance. To note, occasionally there are nuclei of non-viable cells within the lumen of the organoids (e.g. **Figure 4A**). As the aim of this analysis is to measure the displacement and velocity of the migrating epithelial cells, the nuclei of these non-viable cells were excluded from the analysis. The 3D plot of nuclei position was done using scatter3sph v.1.5.0.0 in MATLAB.

**Statistical analysis**

Statistical analyses were conducted using Welch's *t*-test between sample pairs. The analyses were performed using GraphPad Prism v.10. All statistical tests were considered significant if $p < 0.05$. Unless otherwise stated, all plots show mean ± SEM.

**Acknowledgment**

The authors would like to thank the Confocal Microscopy Laboratory at FSU College of Medicine for access to the confocal microscopes. The authors would like to thank Dr. Terra Bradley for the careful editing of the manuscript. JI and GX were supported by startup funds from Florida State University, awards from the Florida Department of Health's Bankhead-Coley Cancer Research Program (award number 21B11), and Live Like Bella Pediatric Cancer Research Initiative (award number 23L06). YJW was supported by the American Diabetes Association grant #11-22-JDFPM-03 and the Islet Award Initiative (IIDP-IAI; https://iidp.coh.org/Investigators/Islet-Award-Initiative). Human pancreatic exocrine tissues were provided by the NIDDK-funded Integrated Islet Distribution Program (IIDP) (RRID:SCR_014387) at City of Hope, NIH Grant # U24DK098085. The PDAC organoid line is from the Human Cancer Models Initiative (HCMI), https://ocg.cancer.gov/programs/HCMI. DT and XL were supported by the National Science Foundation (grant no. PHY 2310639), the Collie-Welch Chair through the Welch Foundation (F-0019).

**Reference**

1. Friedl, P. and D. Gilmour, *Collective cell migration in morphogenesis, regeneration and cancer.* Nat Rev Mol Cell Biol, 2009. **10**(7): p. 445-57

2. Williams, A.M., S. Donoughe, E. Munro, and S. Horne-Badovinac, *Fat2 polarizes the WAVE complex in trans to align cell protrusions for collective migration.* Elife, 2022. **11**.PMC9576270

3. Sherrard, K.M., M. Cetera, and S. Horne-Badovinac, *DAAM mediates the assembly of long-lived, treadmilling stress fibers in collectively migrating epithelial cells in Drosophila.* Elife, 2021. **10**.PMC8610420

4. Popkova, A., O.J. Stone, L. Chen, X. Qin, C. Liu, J. Liu, K. Belguise, D.J. Montell, K.M. Hahn, M. Rauzi, and X. Wang, *A Cdc42-mediated supracellular network drives polarized forces and Drosophila egg chamber extension.* Nat Commun, 2020. **11**(1): p. 1921.PMC7174421

5. Williams, A.M. and S. Horne-Badovinac, *Fat2 polarizes Lar and Sema5c to coordinate the motility of collectively migrating epithelial cells.* J Cell Sci, 2024. **137**(5).PMC10508692

6. Barlan, K., M. Cetera, and S. Horne-Badovinac, *Fat2 and Lar Define a Basally Localized Planar Signaling System Controlling Collective Cell Migration.* Dev Cell, 2017. **40**(5): p. 467-477 e5.PMC5354100

7. Marmaras, A., U. Berge, A. Ferrari, V. Kurtcuoglu, D. Poulikakos, and R. Kroschewski, *A mathematical method for the 3D analysis of rotating deformable systems applied on lumen-forming MDCK cell aggregates.* Cytoskeleton (Hoboken), 2010. **67**(4): p. 224-40

8. Chin, A.S., K.E. Worley, P. Ray, G. Kaur, J. Fan, and L.Q. Wan, *Epithelial Cell Chirality Revealed by Three-Dimensional Spontaneous Rotation.* Proc Natl Acad Sci U S A, 2018. **115**(48): p. 12188-12193.PMC6275504

9. Hirata, E., T. Ichikawa, S.I. Horike, and E. Kiyokawa, *Active K-RAS induces the coherent rotation of epithelial cells: A model for collective cell invasion in vitro.* Cancer Sci, 2018. **109**(12): p. 4045-4055.PMC6272113

10. Hof, L., T. Moreth, M. Koch, T. Liebisch, M. Kurtz, J. Tarnick, S.M. Lissek, M.M.A. Verstegen, L.J.W. van der Laan, M. Huch, F. Matthaus, E.H.K. Stelzer, and F. Pampaloni, *Long-term live imaging and multiscale analysis identify heterogeneity and core principles of epithelial organoid morphogenesis.* BMC Biol, 2021. **19**(1): p. 37.PMC7903752 (US9816916B2).

11. Tan, T.H., A. Amiri, I. Seijo-Barandiaran, M.F. Staddon, A. Materne, S. Tomas, C. Duclut, M. Popović, A. Grapin-Botton, and F. Jülicher, *Emergent chirality in active solid rotation of pancreas spheres.* PRX Life, 2024. **2**(3): p. 033006

12. Tanner, K., H. Mori, R. Mroue, A. Bruni-Cardoso, and M.J. Bissell, *Coherent angular motion in the establishment of multicellular architecture of glandular tissues.* Proc Natl Acad Sci U S A, 2012. **109**(6): p. 1973-8.PMC3277511

13. Wang, H., S. Lacoche, L. Huang, B. Xue, and S.K. Muthuswamy, *Rotational motion during three-dimensional morphogenesis of mammary epithelial acini relates to laminin matrix assembly.* Proc Natl Acad Sci U S A, 2013. **110**(1): p. 163-8.PMC3538193

14. Brandstatter, T., D.B. Bruckner, Y.L. Han, R. Alert, M. Guo, and C.P. Broedersz, *Curvature induces active velocity waves in rotating spherical tissues.* Nat Commun, 2023. **14**(1): p. 1643.PMC10039078

15. Haigo, S.L. and D. Bilder, *Global tissue revolutions in a morphogenetic movement controlling elongation.* Science, 2011. **331**(6020): p. 1071-4.PMC3153412

16. Crest, J., A. Diz-Munoz, D.Y. Chen, D.A. Fletcher, and D. Bilder, *Organ sculpting by patterned extracellular matrix stiffness.* Elife, 2017. **6**.PMC5503509

17. Fernandez, P.A., B. Buchmann, A. Goychuk, L.K. Engelbrecht, M.K. Raich, C.H. Scheel, E. Frey, and A.R. Bausch, *Surface-tension-induced budding drives alveologenesis in human mammary gland organoids.* Nat Phys, 2021. **17**: p. 1130-1136.PMC7612858

18. Lu, L., T. Guyomar, Q. Vagne, R. Berthoz, A. Torres-Sánchez, M. Lieb, C. Martin-Lemaitre, K. van Unen, A. Honigmann, O. Pertz, D. Riveline, and G. Salbreux, *Polarity-driven three-dimensional spontaneous rotation of a cell doublet.* Nature Physics, 2024

19. Lancaster, M.A., M. Renner, C.A. Martin, D. Wenzel, L.S. Bicknell, M.E. Hurles, T. Homfray, J.M. Penninger, A.P. Jackson, and J.A. Knoblich, *Cerebral organoids model human brain development and microcephaly.* Nature, 2013. **501**(7467): p. 373-9.PMC3817409

20. Sato, T., R.G. Vries, H.J. Snippert, M. van de Wetering, N. Barker, D.E. Stange, J.H. van Es, A. Abo, P. Kujala, P.J. Peters, and H. Clevers, *Single Lgr5 stem cells build crypt-villus structures in vitro without a mesenchymal niche.* Nature, 2009. **459**(7244): p. 262-5

21. Boj, S.F., C.I. Hwang, L.A. Baker, Chio, II, D.D. Engle, V. Corbo, M. Jager, M. Ponz-Sarvise, H. Tiriac, M.S. Spector, A. Gracanin, T. Oni, K.H. Yu, R. van Boxtel, M. Huch, K.D.

Rivera, J.P. Wilson, M.E. Feigin, D. Ohlund, A. Handly-Santana, C.M. Ardito-Abraham, M. Ludwig, E. Elyada, B. Alagesan, G. Biffi, G.N. Yordanov, B. Delcuze, B. Creighton, K. Wright, Y. Park, F.H. Morsink, I.Q. Molenaar, I.H. Borel Rinkes, E. Cuppen, Y. Hao, Y. Jin, I.J. Nijman, C. Iacobuzio-Donahue, S.D. Leach, D.J. Pappin, M. Hammell, D.S. Klimstra, O. Basturk, R.H. Hruban, G.J. Offerhaus, R.G. Vries, H. Clevers, and D.A. Tuveson, *Organoid models of human and mouse ductal pancreatic cancer.* Cell, 2015. **160**(1-2): p. 324-38.PMC4334572

22. Kim, J., B.K. Koo, and J.A. Knoblich, *Human organoids: model systems for human biology and medicine.* Nat Rev Mol Cell Biol, 2020. **21**(10): p. 571-584.PMC7339799

23. Corsini, N.S. and J.A. Knoblich, *Human organoids: New strategies and methods for analyzing human development and disease.* Cell, 2022. **185**(15): p. 2756-2769

24. Huch, M., P. Bonfanti, S.F. Boj, T. Sato, C.J. Loomans, M. van de Wetering, M. Sojoodi, V.S. Li, J. Schuijers, A. Gracanin, F. Ringnalda, H. Begthel, K. Hamer, J. Mulder, J.H. van Es, E. de Koning, R.G. Vries, H. Heimberg, and H. Clevers, *Unlimited in vitro expansion of adult bi-potent pancreas progenitors through the Lgr5/R-spondin axis.* EMBO J, 2013. **32**(20): p. 2708-21.PMC3801438

25. Dasgupta, S., K. Gupta, Y. Zhang, V. Viasnoff, and J. Prost, *Physics of lumen growth.* Proc Natl Acad Sci U S A, 2018. **115**(21): p. E4751-E4757.PMC6003502

26. Narayanan, V., L.E. Schappell, C.R. Mayer, A.A. Duke, T.J. Armiger, P.T. Arsenovic, A. Mohan, K.N. Dahl, J.P. Gleghorn, and D.E. Conway, *Osmotic Gradients in Epithelial Acini Increase Mechanical Tension across E-cadherin, Drive Morphogenesis, and Maintain Homeostasis.* Curr Biol, 2020. **30**(4): p. 624-633 e4.PMC7153951

27. Indana, D., A. Zakharov, Y. Lim, A.R. Dunn, N. Bhutani, V.B. Shenoy, and O. Chaudhuri, *Lumen expansion is initially driven by apical actin polymerization followed by osmotic pressure in a human epiblast model.* Cell Stem Cell, 2024. **31**(5): p. 640-656 e8.PMC11323070

28. Kovacs, M., J. Toth, C. Hetenyi, A. Malnasi-Csizmadia, and J.R. Sellers, *Mechanism of blebbistatin inhibition of myosin II.* J Biol Chem, 2004. **279**(34): p. 35557-63

29. Vinzenz, M., M. Nemethova, F. Schur, J. Mueller, A. Narita, E. Urban, C. Winkler, C. Schmeiser, S.A. Koestler, K. Rottner, G.P. Resch, Y. Maeda, and J.V. Small, *Actin*

*branching in the initiation and maintenance of lamellipodia.* J Cell Sci, 2012. **125**(Pt 11): p. 2775-85

30. Squarr, A.J., K. Brinkmann, B. Chen, T. Steinbacher, K. Ebnet, M.K. Rosen, and S. Bogdan, *Fat2 acts through the WAVE regulatory complex to drive collective cell migration during tissue rotation.* J Cell Biol, 2016. **212**(5): p. 591-603.PMC4772498

31. Nolen, B.J., N. Tomasevic, A. Russell, D.W. Pierce, Z. Jia, C.D. McCormick, J. Hartman, R. Sakowicz, and T.D. Pollard, *Characterization of two classes of small molecule inhibitors of Arp2/3 complex.* Nature, 2009. **460**(7258): p. 1031-4.PMC2780427

32. Mullins, R.D., J.A. Heuser, and T.D. Pollard, *The interaction of Arp2/3 complex with actin: nucleation, high affinity pointed end capping, and formation of branching networks of filaments.* Proc Natl Acad Sci U S A, 1998. **95**(11): p. 6181-6.PMC27619

33. Yang, E.Y. and H.L. Moses, *Transforming growth factor beta 1-induced changes in cell migration, proliferation, and angiogenesis in the chicken chorioallantoic membrane.* J Cell Biol, 1990. **111**(2): p. 731-41.PMC2116177

34. Xu, J., S. Lamouille, and R. Derynck, *TGF-beta-induced epithelial to mesenchymal transition.* Cell Res, 2009. **19**(2): p. 156-72.PMC4720263

35. Chan, C.J., M. Costanzo, T. Ruiz-Herrero, G. Monke, R.J. Petrie, M. Bergert, A. Diz-Munoz, L. Mahadevan, and T. Hiiragi, *Hydraulic control of mammalian embryo size and cell fate.* Nature, 2019. **571**(7763): p. 112-116

36. Chan, C.J. and T. Hiiragi, *Integration of luminal pressure and signalling in tissue self-organization.* Development, 2020. **147**(5)

37. Bagnat, M., B. Daga, and S. Di Talia, *Morphogenetic Roles of Hydrostatic Pressure in Animal Development.* Annu Rev Cell Dev Biol, 2022. **38**: p. 375-394.PMC9675319

38. Schamberger, B., R. Ziege, K. Anselme, M. Ben Amar, M. Bykowski, A.P.G. Castro, A. Cipitria, R.A. Coles, R. Dimova, M. Eder, S. Ehrig, L.M. Escudero, M.E. Evans, P.R. Fernandes, P. Fratzl, L. Geris, N. Gierlinger, E. Hannezo, A. Iglič, J.J.K. Kirkensgaard, P. Kollmannsberger, Ł. Kowalewska, N.A. Kurniawan, I. Papantoniou, L. Pieuchot, T.H.V. Pires, L.D. Renner, A.O. Sageman-Furnas, G.E. Schröder-Turk, A. Sengupta, V.R. Sharma, A. Tagua, C. Tomba, X. Trepat, S.L. Waters, E.F. Yeo, A. Roschger, C.M. Bidan, and J.W.C. Dunlop, *Curvature in Biological Systems: Its Quantification, Emergence, and Implications across the Scales.* Advanced Materials, 2023. **35**(13): p. 2206110

39. Ershov, D., M.-S. Phan, J.W. Pylvänäinen, S.U. Rigaud, L. Le Blanc, A. Charles-Orszag, J.R.W. Conway, R.F. Laine, N.H. Roy, D. Bonazzi, G. Duménil, G. Jacquemet, and J.-Y. Tinevez, *TrackMate 7: integrating state-of-the-art segmentation algorithms into tracking pipelines.* Nature Methods, 2022. **19**(7): p. 829-832

40. Schmidt, U., M. Weigert, C. Broaddus, and G. Myers. *Cell Detection with Star-Convex Polygons*. in *Medical Image Computing and Computer Assisted Intervention – MICCAI 2018*. 2018. Cham: Springer International Publishing.

41. Schindelin, J., I. Arganda-Carreras, E. Frise, V. Kaynig, M. Longair, T. Pietzsch, S. Preibisch, C. Rueden, S. Saalfeld, B. Schmid, J.Y. Tinevez, D.J. White, V. Hartenstein, K. Eliceiri, P. Tomancak, and A. Cardona, *Fiji: an open-source platform for biological-image analysis.* Nat Methods, 2012. **9**(7): p. 676-82.PMC3855844

42. Crocker, J.C. and D.G. Grier, *Methods of Digital Video Microscopy for Colloidal Studies.* Journal of Colloid and Interface Science, 1996. **179**(1): p. 298-310

# Figure 1

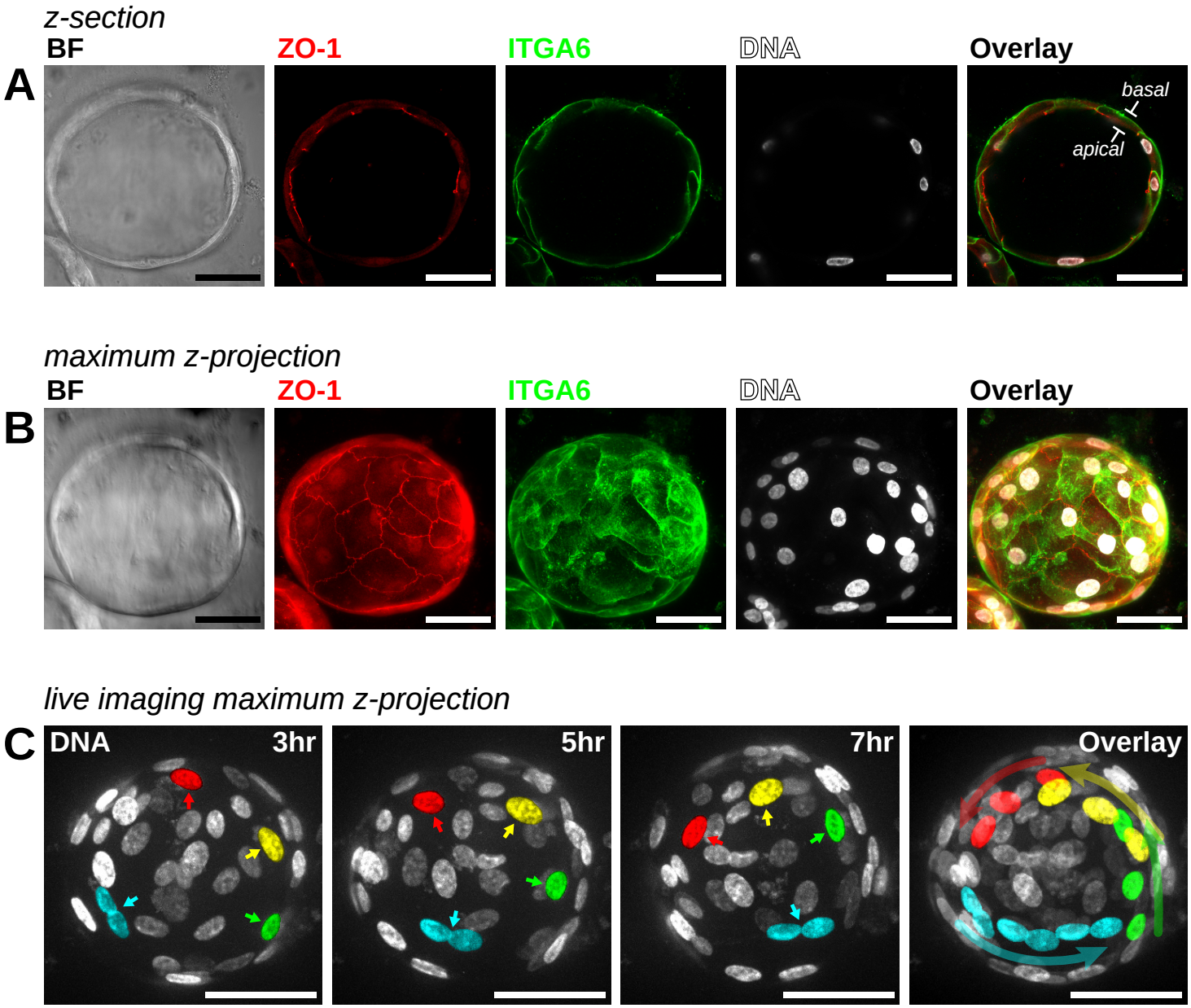
z-section
A
BF
ZO-1
ITGA6
DNA
Overlay
basal
apical
maximum z-projection
B
BF
ZO-1
ITGA6
DNA
Overlay
live imaging maximum z-projection
C
DNA
3hr
5hr
7hr
Overlay

**Figure 1. Rotational migration of the human pancreatic ductal organoid.**

**(A)** Confocal section taken at the middle of a human pancreatic ductal organoid showing the cystic morphology of the organoid, a lumen encapsulated by a layer of pancreatic ductal epithelial cells. The organoids retain their apical-basal polarity as shown by the apical marker protein ZO-1 at the lumen side (inside) and the basal marker protein ITGA6 at the organoid interface with the Matrigel (outside). Bar = 50 µm.

**(B)** Maximum projection of the confocal sections taken from the pancreatic ductal organoid, showing the continuous staining of the tight junction protein ZO-1 between the ductal cells, the distribution of the integrin protein ITGA6 at the basal side of the cells, and the distribution of nuclei within the organoid. Bar = 50 µm.

**(C)** Maximum projection of confocal sections taken during the live imaging of pancreatic ductal organoid nuclei, showing the rotational migration of the organoid. Pseudo-colors (red, yellow, green, and cyan) were assigned to several nuclei to illustrate the location of these nuclei over time. Bar = 50 µm.

# Figure 2

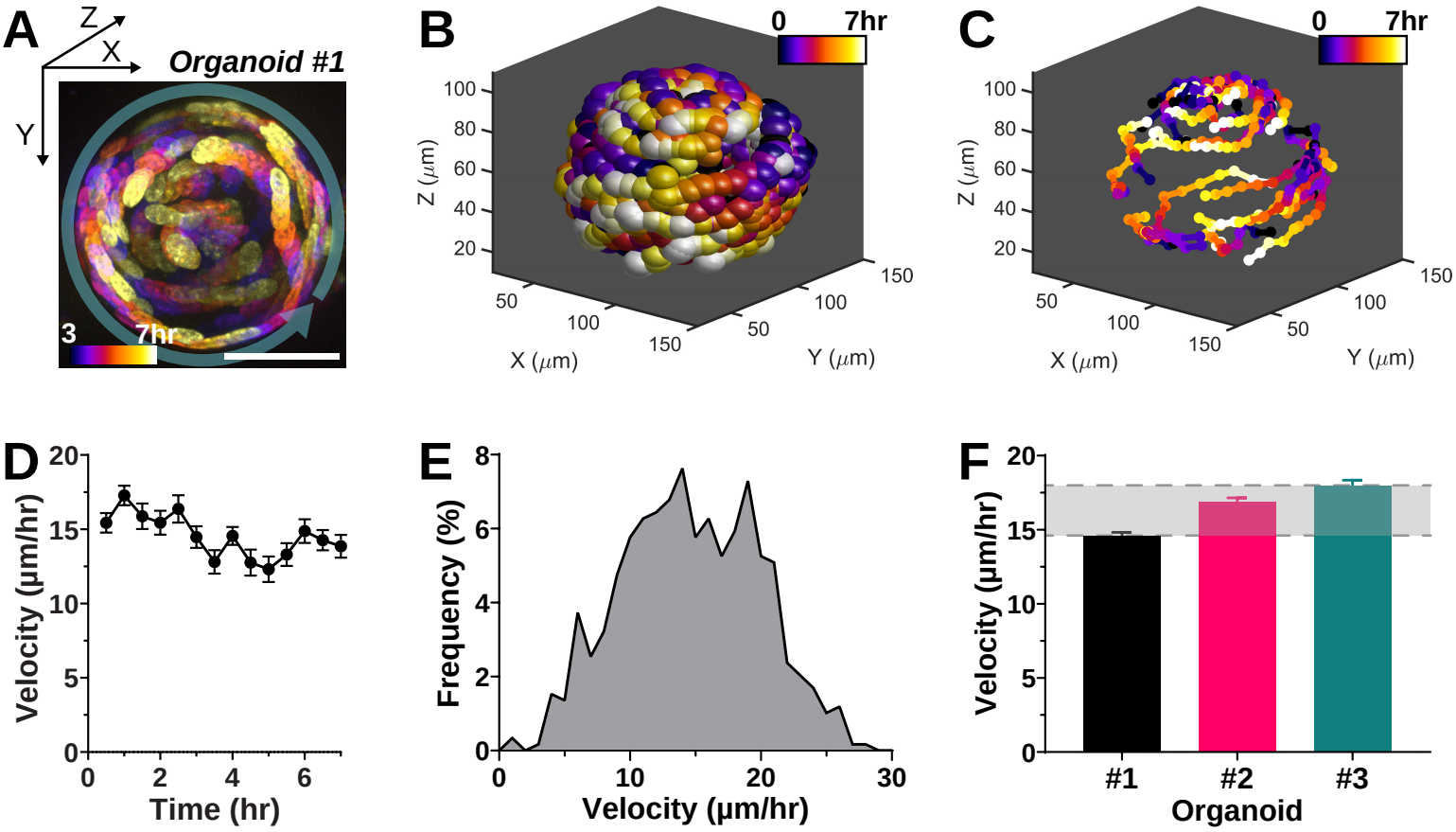
A
Z
X
Y
Organoid #1
3
7hr
B
0
7hr
Z (μm)
X (μm)
Y (μm)
C
0
7hr
Z (μm)
X (μm)
Y (μm)
D
Velocity (μm/hr)
Time (hr)
E
Frequency (%)
Velocity (μm/hr)
F
Velocity (μm/hr)
#1
#2
#3
Organoid

**Figure 2. Trajectory and velocity of pancreatic ductal organoid rotation.**

**(A)** Overlay of maximum projections of a rotating pancreatic ductal organoid taken every 30 minutes, between hours 3 and 7 of the live imaging. To illustrate the rotational migration of the cells, the nuclei were color-coded based on the time point they were imaged. The transparent green arrow indicates the general direction of the rotation. The x and y position coordinates start from the top left of the image. Bar = 50 µm.

**(B)** Three-dimensional reconstruction of the nuclei position over time.

**(C)** Trajectories of the nuclei within the rotating organoid.

**(D)** The velocity of each nucleus at each time point was calculated from the displacement covered between time points. The nuclei average velocity remains relatively stable at ~15 µm/hr over the imaging period.

**(E)** Histogram plot showing the distribution of the recorded velocity. The velocity ranges between 0 to 30 µm/hr, with a peak at ~15 µm/hr.

**(F)** Average velocity of three independent pancreatic ductal organoids, showing a range between ~15 and ~18 µm/hr (mean±SEM).

# Figure 3

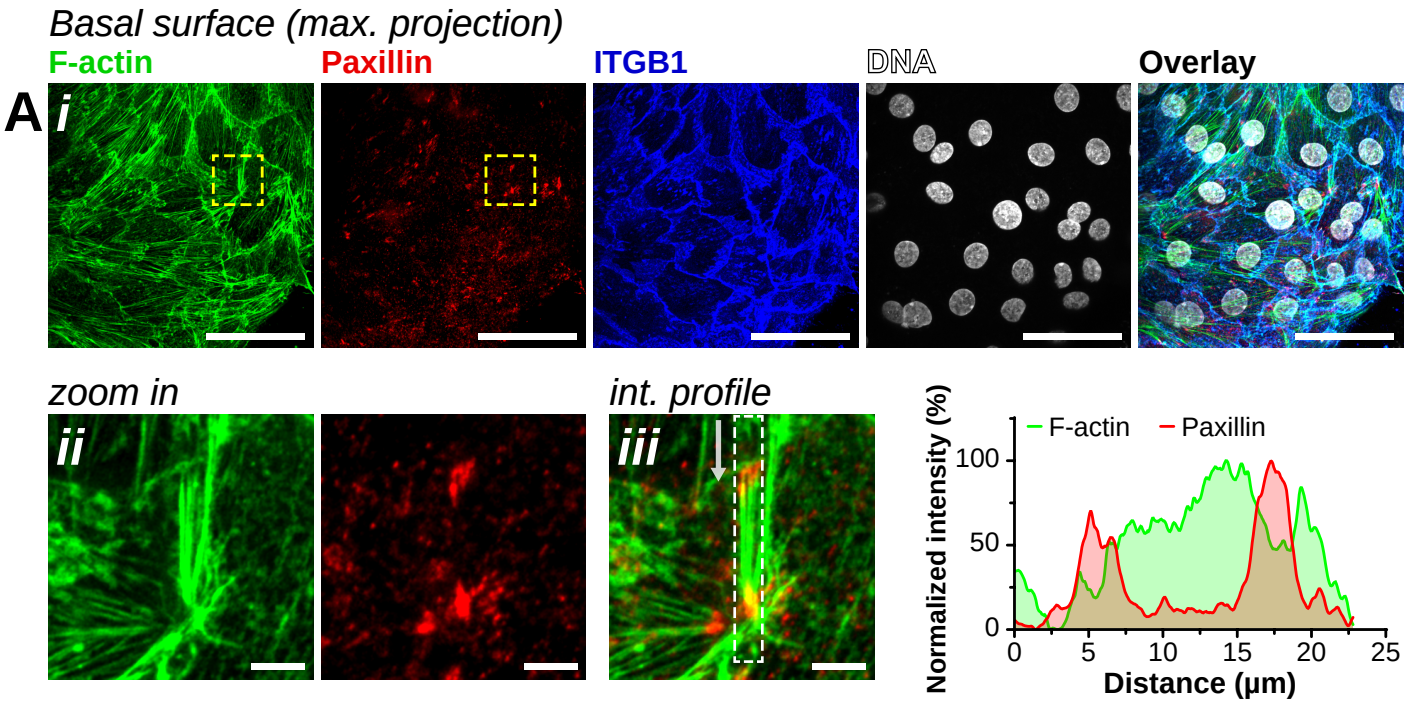
Basal surface (max. projection)
F-actin
Paxillin
ITGB1
DNA
Overlay
A
i
zoom in
ii
int. profile
iii
F-actin
Paxillin
Normalized intensity (%)
100
50
0
0
5
10
15
20
25
Distance (µm)

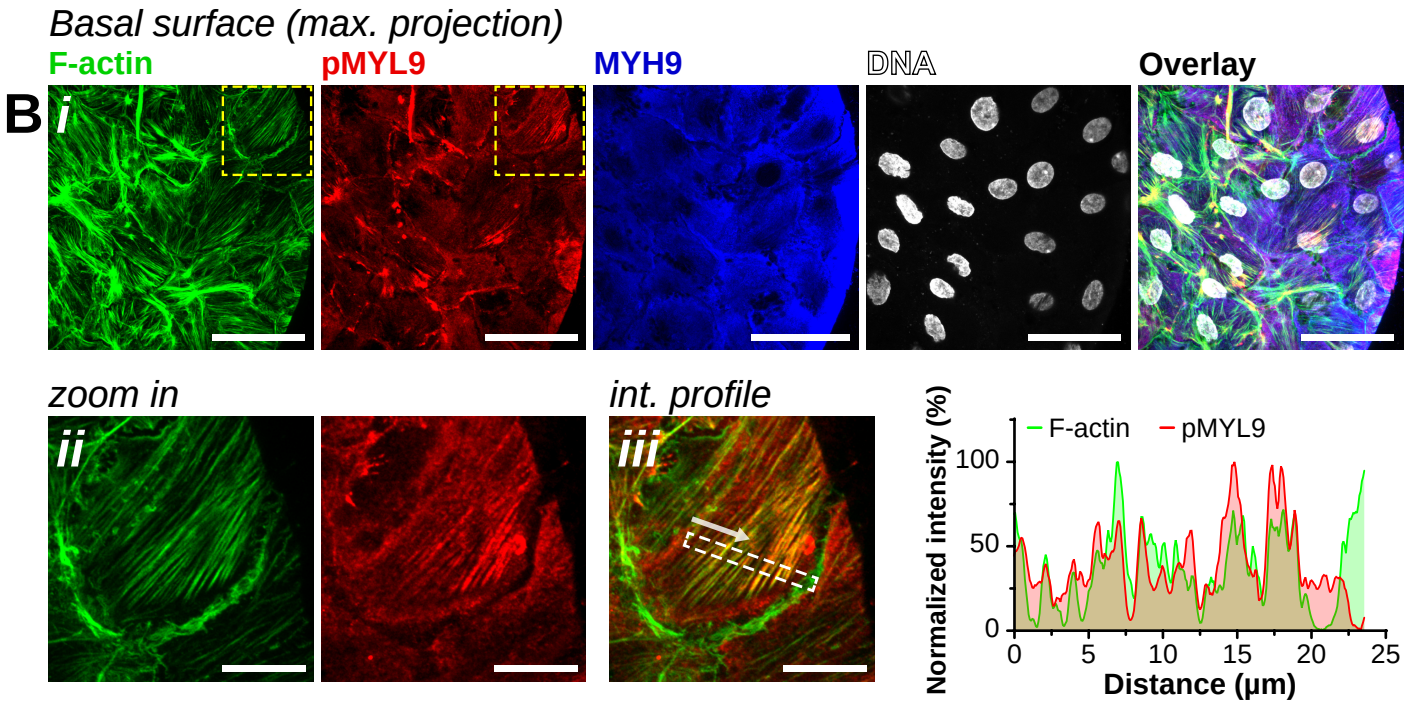
Basal surface (max. projection)
F-actin
pMYL9
MYH9
DNA
Overlay
B
i
zoom in
ii
int. profile
iii
F-actin
pMYL9
Normalized intensity (%)
100
50
0
0
5
10
15
20
25
Distance (µm)

**Figure 3. Actin stress fibers, focal adhesion, and phosphorylated myosin at the basal side of the pancreatic ductal organoid.**

**(A) (i)** Confocal maximum projection of the basal surface of pancreatic ductal organoid stained for filamentous actin (F-actin), focal adhesion protein paxillin, integrin β1 (ITGB1), and DNA. Prominent actin stress fibers and clusters of focal adhesion protein, paxillin, were observed at the basal surface. Bar = 50 µm. **(ii-iii)** Zoomed-in images from the yellow dash boxes of **Figure 3A(i)** and intensity profile showing the location of paxillin clusters at the end of the stress fibers. The white arrow indicates the direction of the intensity profile and the white dash box indicates the area used to derive the intensity profile. Bar = 5 µm.

**(B) (i)** Confocal maximum projection of the basal surface of pancreatic ductal organoid stained for F-actin, phosphorylated myosin light chain 9 (pMYL9), non-muscle myosin heavy chain 9 (MYH9), and DNA. Colocalization of F-actin and pMYL9 was observed in some of the stress fibers. Bar = 50 µm. **(ii-iii)** Zoomed-in images from the yellow dash boxes of **Figure 3B(i)** and intensity profile confirm the colocalization of actin stress fibers and pMYL9. The white arrow indicates the direction of the intensity profile and the white dash box indicates the area used to derive the intensity profile. Bar = 15 µm.

# Figure 4

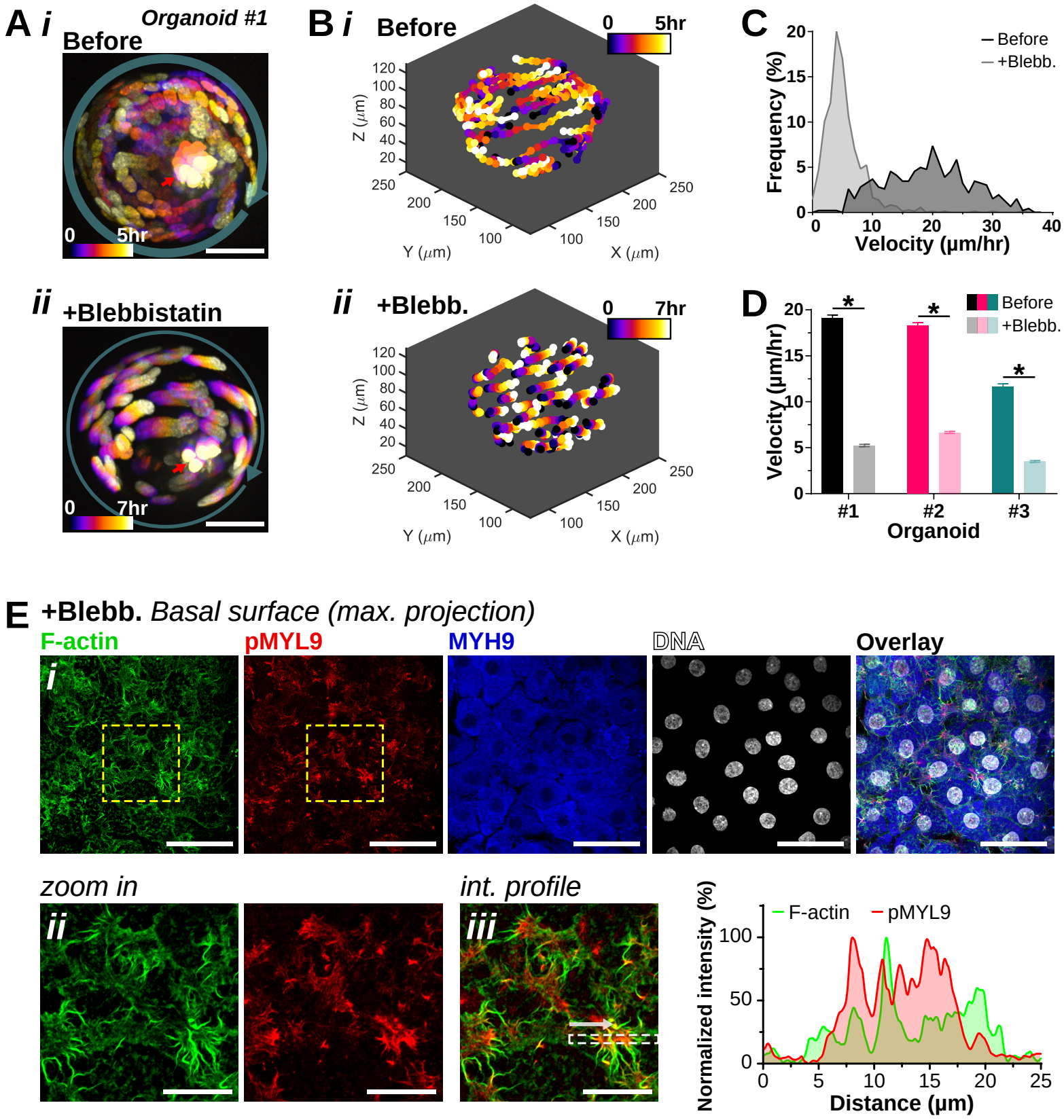
A i
Organoid #1
Before
0
5hr
ii
+Blebbistatin
0
7hr
B i
Before
0
5hr
Z (μm)
Y (μm)
X (μm)
ii
+Blebb.
0
7hr
C
Frequency (%)
Velocity (μm/hr)
Before
+Blebb.
D
Velocity (μm/hr)
Organoid
#1
#2
#3
Before
+Blebb.
E
+Blebb. Basal surface (max. projection)
F-actin
pMYL9
MYH9
DNA
Overlay
i
zoom in
ii
int. profile
iii
Normalized intensity (%)
Distance (μm)
F-actin
pMYL9

**Figure 4. Inhibition of myosin activity disrupts pancreatic ductal organoid rotation and actin stress fibers.**

**(A) (i)** Overlay of maximum projections of a rotating pancreatic ductal organoid taken before the myosin inhibitor, Blebbistatin, treatment. The images were taken every 30 minutes for 5 hours. The transparent green arrow indicates the general direction of the rotation. Bar = 50 µm. **(ii)** Overlay of maximum projections of the same organoid taken 1 hour after the 200 µM Blebbistatin treatment, showing the significant slowdown of the rotation. The images were taken every 30 minutes for 7 hours. Bar = 50 µm. The nuclei were color-coded based on the time when they were taken. The red arrow points to the nuclei of non-viable cells within the lumen of the organoid, which are excluded from the subsequent nucleus tracking analyses.

**(B)** The nuclei trajectory of the corresponding pancreatic ductal organoid before **(i)** and after **(ii)** Blebbistatin treatment.

**(C)** Histogram plot showing the velocity distribution of the nuclei before and after the Blebbistatin treatment. The plot shows the decrease in cell velocity after Blebbistatin treatment.

**(D)** Average velocity of three independent pancreatic ductal organoids before and after the Blebbistatin treatment. The decrease in velocity was observed in all three organoids (mean±SEM, $*p < 0.0001$).

**(E) (i)** Confocal maximum projection of the basal surface of pancreatic ductal organoid treated with 200 µM Blebbistain for 12 hr and stained for F-actin, pMYL9, MYH9, and DNA. Bar = 50 µm. **(ii-iii)** Zoomed-in images and intensity profile showing the disrupted actin stress fibers and the accumulation of pMYL9 at the base of the stress fibers. The white arrow indicates the direction of the intensity profile and the white dash box indicates the area used to derive the intensity profile. Bar = 20 µm.

# Figure 5

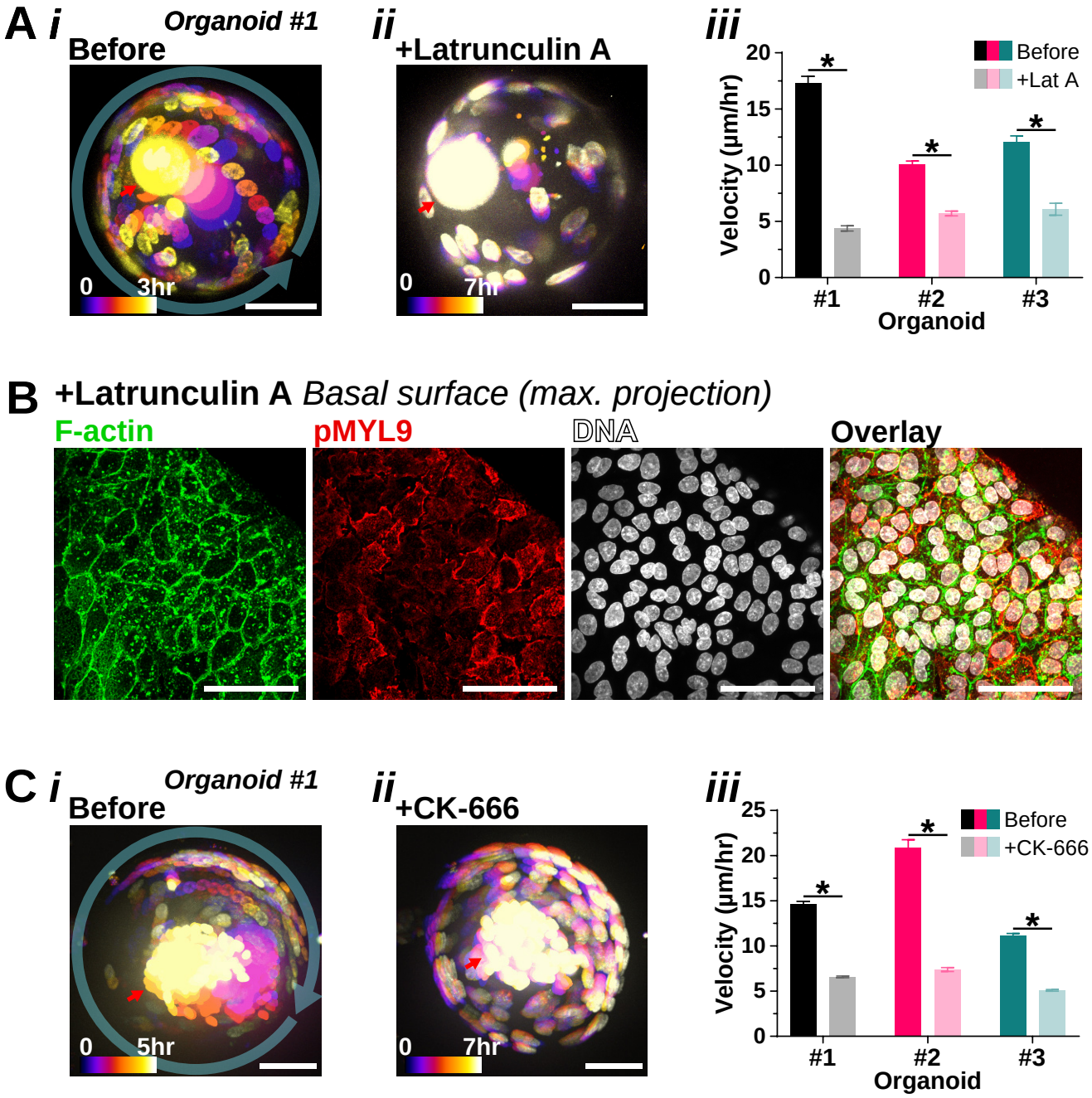
A i
Organoid #1
Before
0
3hr
ii
+Latrunculin A
0
7hr
iii
Before
+Lat A
Velocity (µm/hr)
20
15
10
5
0
*
*
*
#1
#2
#3
Organoid
B +Latrunculin A Basal surface (max. projection)
F-actin
pMYL9
DNA
Overlay
C i
Organoid #1
Before
0
5hr
ii
+CK-666
0
7hr
iii
Before
+CK-666
Velocity (µm/hr)
25
20
15
10
5
0
*
*
*
#1
#2
#3
Organoid
D +CK-666 Basal surface (max. projection)
F-actin
pMYL9
DNA
Overlay

**Figure 5. Inhibition of actin polymerization and branching also disrupt pancreatic ductal organoid rotation.**

**(A) (i)** Overlay of maximum projections of a rotating pancreatic ductal organoid taken before the actin polymerization inhibitor, Latrunculin A, treatment. The images were taken every 30 minutes for 3 hours. The transparent green arrow indicates the general direction of the rotation. Bar = 50 µm. **(ii)** Overlay of maximum projections of the same organoid taken 1 hour after the 1 µM Latrunculin A treatment, showing the significant slowdown of the rotation. The images were taken every 30 minutes for 7 hours. Bar = 50 µm. The nuclei were color-coded based on the time when they were taken. The red arrow points to the nuclei of non-viable cells within the lumen of the organoid, which are excluded from the subsequent nucleus tracking analyses. **(iii)** Average velocity of three independent pancreatic ductal organoids before and after the Latrunculin A treatment. The decrease in velocity was observed in all three organoids (mean±SEM, $*p < 0.0001$).

**(B)** Confocal maximum projection of the basal surface of pancreatic ductal organoid treated with 1 µM Latrunculin A for 12 hr and stained for F-actin, pMYL9, and DNA. Actin polymerization inhibition by Latrunculin A resulted in the total disassembly of actin stress fibers and prominent cortical actin distribution was observed around the perimeter of each cell. Accumulation of pMYL9 was also observed at the perimeter of the cells. Bar = 50 µm.

**(C) (i)** Overlay of maximum projections of a rotating pancreatic ductal organoid taken before the actin branching complex Arp2/3 inhibitor, CK-666, treatment. The images were taken every 30 minutes for 5 hours. The transparent green arrow indicates the general direction of the rotation. Bar = 50 µm. **(ii)** Overlay of maximum projections of the same organoid taken 1 hour after the 200 µM CK-666 treatment, showing the significant slowdown of the rotation. The images were taken every 30 minutes for 7 hours. Bar = 50 µm. The nuclei were color-coded based on the time when they were taken. The red arrow points to the nuclei of non-viable cells within the lumen of the organoid, which are excluded from the subsequent nucleus tracking analyses. **(iii)** Average velocity of three independent pancreatic ductal organoids before and after the CK-666 treatment. The decrease in velocity was observed in all three organoids (mean±SEM, $*p < 0.0001$).

**(D)** Confocal maximum projection of the basal surface of pancreatic ductal organoid treated with 200 µM CK-666 for 12 hr and stained for F-actin, pMYL9, and DNA. Actin stress fibers were still observed after actin branching inhibition by CK-666, and some of the fibers were decorated with the active pMYL9. This suggests the importance of actin branching for the organoid rotational migration. Bar = 50 µm.